Electrochimica Acta 55 (2010) 3537–3541

Contents lists available at ScienceDirect

Electrochimica Acta

journal homepage: www.elsevier.com/locate/electacta

Preparation and characterization of three-dimensional tin thin-film anode with good cycle performance

Zhijia Du, Shichao Zhang*, Tao Jiang, Zhiming Bai

School of Materials Science and Engineering, Beihang University, Xueyuan Road, Haidian District, Beijing 100191, PR China

ARTICLE INFO

Article history:
Received 17 November 2009
Received in revised form 14 January 2010
Accepted 17 January 2010
Available online 25 January 2010

Keywords:
Lithium-ion battery
Tin anode
Thin film
Three-dimension
Electroless plating

ABSTRACT

Three-dimensional tin thin-film anode was prepared by electroless plating tin onto three-dimensional (3D) copper foam (which served as current collector), and characterized physically by SEM, EDS and XRD. Its electrochemical property and mechanism were studied by charge–discharge test, cyclic voltammetry (CV) and electrochemical impedance spectroscopy (EIS). The SEM and EDS results indicated that tin film with 500 nm thickness was formed over the whole surface of copper branches. The XRD results suggested that a new phase of Cu_6Sn_5 was formed between copper and tin. Besides the tin microflake structure of 500 nm thickness, the interaction effects of the copper foam and Cu_6Sn_5 phase formed between copper and tin resulted in good cycle performance with first discharge capacity of 737 mAh g^{-1}, 97% capacity retention after 20 cycles and still 84% after 40 cycles.

1. Introduction

As a successful application in lithium-ion batteries, carbonaceous materials have many advantages such as stable charge–discharge properties and low-cost [1]. However, since their theoretical capacity is only 372 mAh g^{-1}, it is important to develop new anode materials with higher capacity. Sn and Li can form $Li_{4.4}Sn$ in lithiation process with theoretical capacity of 994 mAh g^{-1}, which has attracted researchers' interest [2]. Previously, people carried out many methods to prepare tin such as rolling tin pieces to foil, wire electric explosion, constant current electrodeposition, pulse electrodeposition, spray pyrolysis, etc. [3–8]. In these reports, however, severe volume expansion occurred due to lithiation/delithiation process during charge–discharge cycles. Tin gradually cracked, pulverized and shed from the current collector, which caused poor cycle performance and inhibited its application in lithium-ion batteries.

In order to enhance the cyclability of active materials, 3D substrates were used as current collectors, such as carbon paper, nickel foam, copper foam, and copper cellular architecture [9–13]. Compared to compact metal, the foamy metal possesses several advantages. Firstly, it offers a good conductive environment for the active materials. Moreover, its stress absorbability is beneficial to construct a stretchy electrode system which would insure good combination between the active materials and the substrate for preventing the electrode failure [14].

Simultaneously, in order to control the severe volume change, some researchers dispersed tin into inactive components to form the active/inactive system and strengthen the interfacial binding force, such as Sn–Cu, Sn–Ni, Sn–Co, Sn–Mo, Sn–C, etc. [8,15–19]. In Tamura's study, the capacity retention after 10 cycles was improved from 20% to 94% due to the formation of tin–copper intermetallic layers between copper and tin layers by heat treatment which enhanced the interface strength [20]. Although two- or multi-component alloys improved the battery's cyclability to some extent, they are still far from commercialization.

In the present work, copper foam was used as current collector. The electrode was prepared by electroless plating tin onto copper foam. Electroless tin plating is a replacement reaction. Eventually, the good electrochemical behavior of the electrode and the probable mechanism are discussed.

2. Experimental

2.1. Preparation and characterization of the 3D tin thin-film anode

The copper foam was fabricated by electrodepositing copper onto the PU (polyurethane) foam template. And then the PU template was burnt out. In this process, copper foam became brittle and was partially oxidized. Subsequently, the resulting copper foam was heat treated at 700 °C for 1 h under hydrogen/nitrogen (vol.% = 1:3) mixed gas protection.

* Corresponding author. Tel.: +86 10 82338148; fax: +86 01 82339319.
E-mail address: csc@buaa.edu.cn (S. Zhang).

0013-4686/$ – see front matter © 2010 Elsevier Ltd. All rights reserved.
doi:10.1016/j.electacta.2010.01.065

The 3D tin thin-film anodes (named 3D-TTA) were prepared by electroless plating tin onto copper foam at 45 °C for 45 min. The plating bath contained 0.1 M $SnSO_4$, 1 M thiourea, 0.5 M sodium hypophosphite and 0.85 M concentrated sulfuric acid. For comparison, 2D tin thin-film anodes (named 2D-TTA) were also prepared by electroless plating tin onto flat copper foil under the same conditions. All of the electrodes were dried at 60 °C for 60 min in vacuum. The loading mass of tin on copper foam and flat copper foil was 2.9 and 1.1 mg cm^{-2} respectively.

The morphologies, composition and phase structure of electrodes were investigated by field emission scanning electron microscopy (FE-SEM, Hitachi S-4800 SEM system), Hitachi S-530 SEM and MAC Science X-ray diffraction (Cu Kα radiation), respectively.

2.2. Cell assemble and electrochemical measurements

Electrochemical charge–discharge behaviors were investigated in simulant cells assembled with the as-prepared anode, lithium foil and Celgard 2300 membrane in an Ar-filled glove box. 1 M $LiPF_6$/EC-DEC (1:1 by vol.) was used as the electrolyte. All cells were galvanostatically charged and discharged in a battery test system (NEWARE BTS-610, Neware Technology Co., Ltd., China) for a cut-off potential of 0.02–1.5 V (vs. Li/Li^+) at ambient temperature.

CV test was performed between 0 and 2.0 V (vs. Li/Li^+) at 0.2 mV s^{-1}. After the electrodes were charged up to 1.5 V (vs. Li/Li^+), then left on open-circuit for 2 h to obtain equilibrium, EIS measurements were carried out over frequency range from 60 kHz to 10 mHz with ac amplitude of 5 mV. CV and EIS were performed using an electrochemical measurement unit (PARStat 2273).

3. Results and discussion

The copper foam is composed of many hollow branches with rough surface (seen in Fig. 1a) with the sectional image of branch shown in inset of Fig. 1a. Fig. 1b and c shows the cross-section morphology of 3D-TTA prepared by electroless plating tin onto the copper foam. The element composition of 3D-TTA is investigated by EDS as shown in Fig. 1d, which demonstrates the presence of Sn and Cu without other element. The sectional SEM image in Fig. 1b and the spectrograms of points A and B in Fig. 1d suggest that there are deposits overlaid both inside and outside copper branches: tin is deposited everywhere wetted by solution due to the electroless plating. Fig. 1c shows the tin film outside is around 500 nm thick with a dense microstructure.

The charge–discharge curves of 3D-TTA shown in Fig. 2a suggest a poor efficiency during the first cycle with 737 mAh g^{-1} initial discharge capacity and 72% columbic efficiency, which is assigned to the compact microstructure of tin film which severely hinders the lithiation/delithiation process. Besides, the irreversible capacity above 0.8 V is attributed to the decomposition of the electrolyte. In the following cycles, charge–discharge curves have the same profile with good cyclability and efficiency. Fig. 2b shows CV of 3D-TTA at 0.2 mV s^{-1}. A small shoulder at ~0.63 V followed by a sharp peak at ~0.19 V is observed during Li intercalation while a small hump at ~0.40 V accompanied by a huge peak divided into two anodic peaks at ~0.75 and ~0.87 V is observed during Li de-intercalation. The 1st and 2nd cycles have the same CV profile except an irreversible peak at 1.13 V assigned to the decomposition of the electrolyte and SEI formation [21].

Fig. 2c shows the cycling behavior of anodes with current density of 0.75 mA mg^{-1} (=0.75C rate), indicating that 3D-TTA possesses good capacity and efficiency cycling performance while

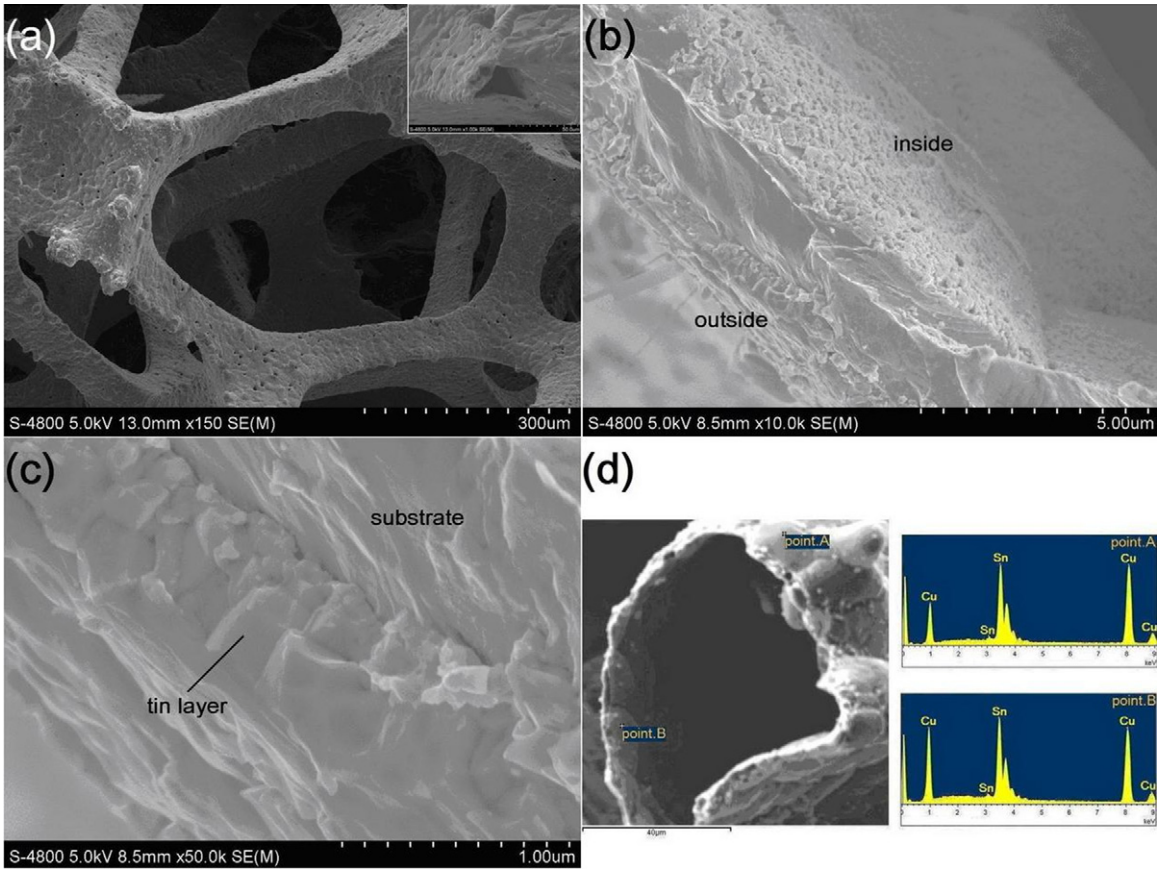

Fig. 1. (a): SEM images of copper foam; (b) and (c): cross-section view of electroless plated 3D-TTA; (d): EDS spectrograms of 3D-TTA.

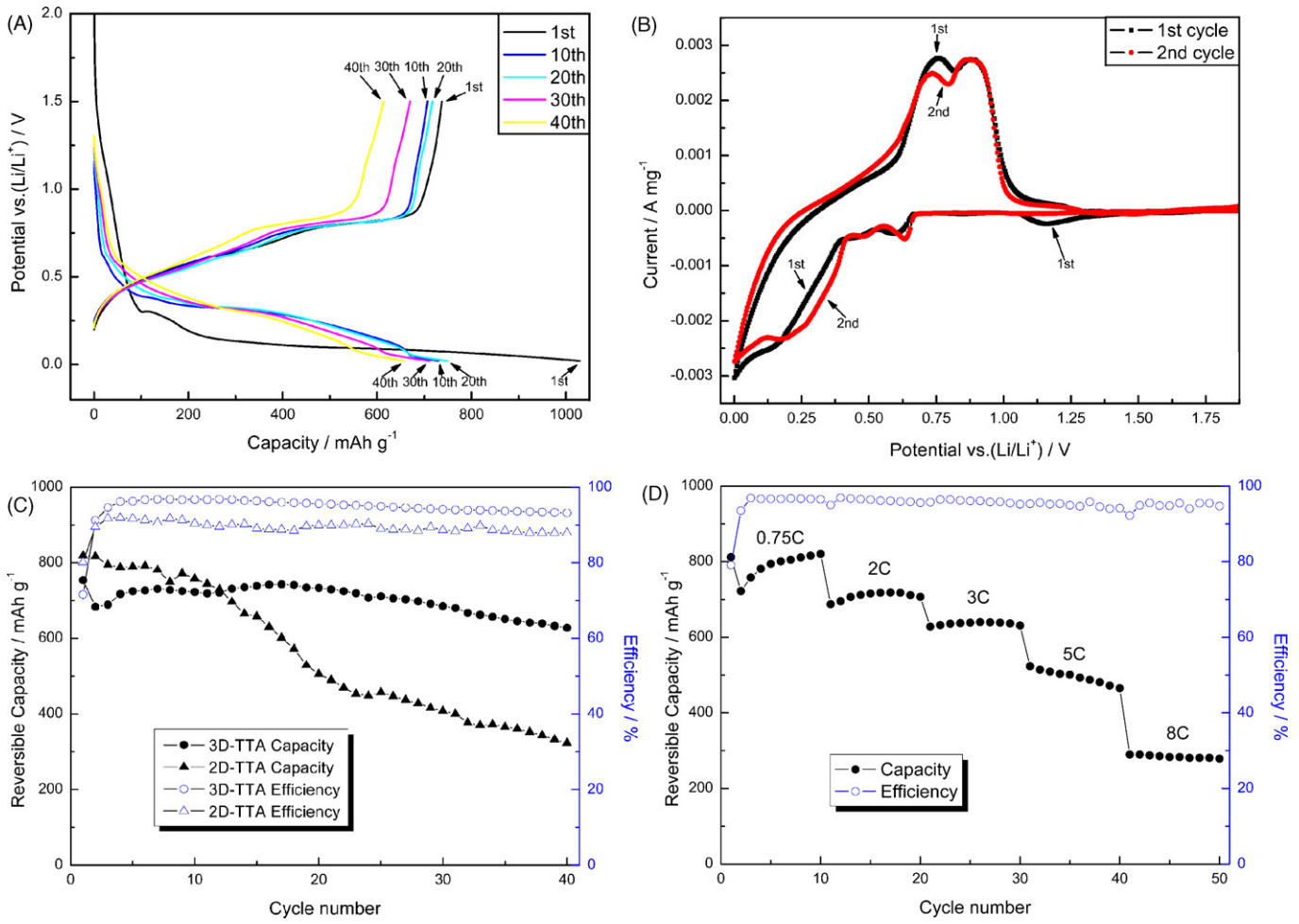

Fig. 2. (a): Galvanostatic charge–discharge curves of 3D-TTA at 0.75C charge–discharge rate; (b): cyclic voltammetry of 3D-TTA at 0.2 mV s^{-1}; (c): capacity and efficiency cycling performance of as-deposited anodes at 0.75C charge–discharge rate; (d): capacity and efficiency cycling performance of 3D-TTA at different charge–discharge rates.

2D-TTA shows poor cyclability and efficiency after the first 10 cycles. The reversible capacity retention of 3D-TTA reaches 97% after 20 cycles, 91% after 30 cycles and still 84% after 40 cycles which is higher than 2D-TTA and other batteries with as-prepared tin anode ever reported. The average columbic efficiency of 3D-TTA is above 95% in the second and following cycles. Fig. 2d shows the high rate capability of 3D-TTA. The charge–discharge rate was increased stepwise up to 8C. The reversible capacity in the first cycle at each rate are 812, 688, 628, 523, 290 mAh g^{-1}, respectively. Compared to the first cycle at each rate, reversible capacity retention after 10 cycles reaches 101%, 103%, 100%, 89%, 96%, respectively. The average columbic efficiency is above 95% at 2C and higher rate.

The SEM micrographs of 3D-TTA and 2D-TTA after 40 galvanostatical charge–discharge cycles were shown in Fig. 3a and b respectively. On the rough surface of the copper branches, tin film cracks gradually and forms microflake structure after 40 cycles

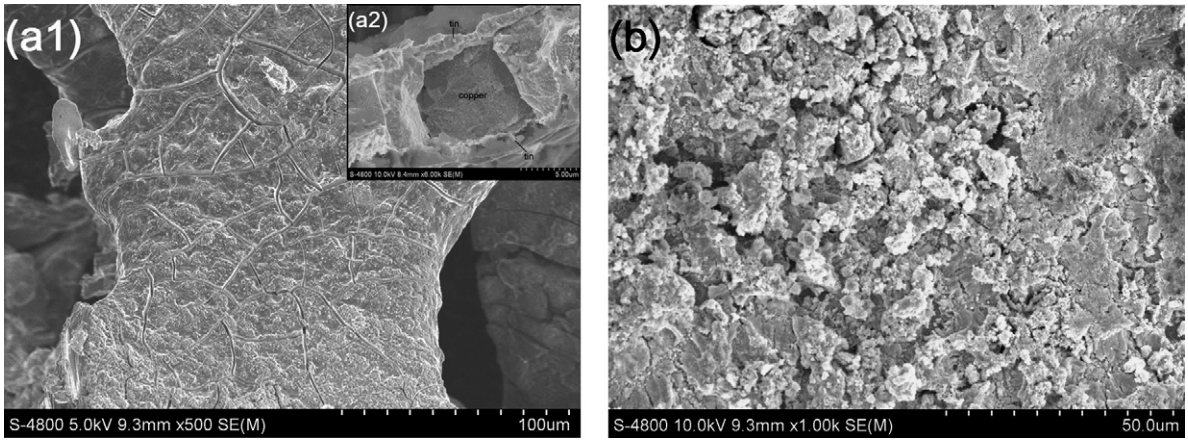

Fig. 3. SEM images of the electrodes after 40 cycles at 0.75C charge–discharge rate. (a1) and (a2): top and cross-section views of 3D-TTA; (b): top view of 2D-TTA.

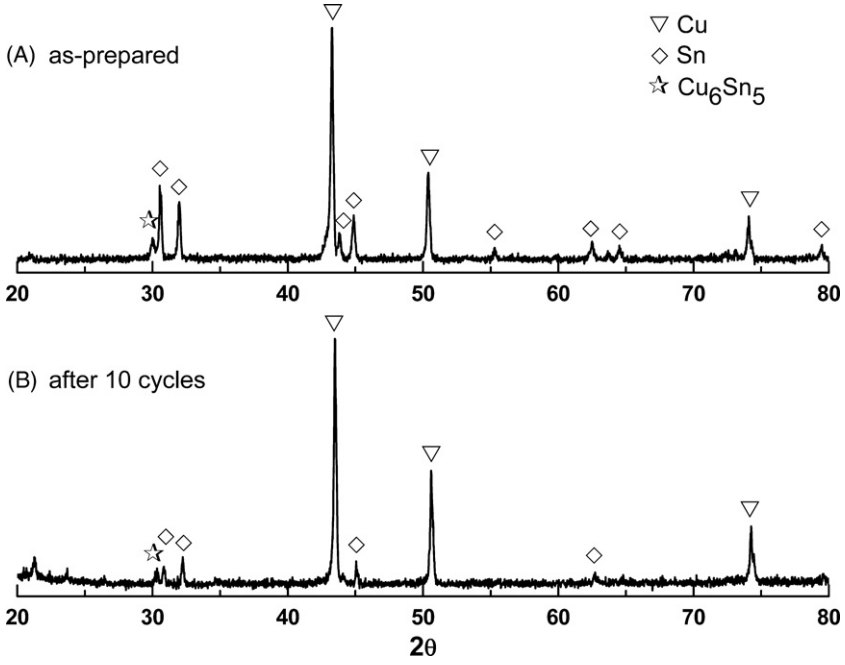

Fig. 4. XRD patterns of 3D-TTA. A: as-prepared; B: after 10 cycles.

(shown in Fig. 3a1). Fig. 3a1 also shows that repeated lithiation/delithiation process causes some pulverization but nearly no shedding. The cross-section morphology in Fig. 3a2 shows that both the inside and outside tin films are retained in 3D-TTA after cyclic volume changes. However, the tin film on flat copper foil emerged severe pulverization and shed from the substrate under cyclic charge–discharge as shown in Fig. 3b.

XRD pattern of 3D-TTA is shown in Fig. 4, which indicates the presence of two basic phases: the main deposited product β-Sn and Cu substrate. The peak at 30.2° is assigned to (1 0 1) plane of Cu_6Sn_5 phase with minor quantity. In electroless plating solution, the potential of $[Cu(NH_2CSNH_2)_4]^{2+}$/Cu redox pair is more negative than Sn^{2+}/Sn redox pair. This leads to copper dissolving while tin is plating on current collector and finally a layer of Cu_6Sn_5 is formed along the interface. The formation of Cu_6Sn_5 layer enhances the bonding force between active materials and current collector, which restrains tin's shedding from the current collector and leads to good cycling performance. Accordingly, the cyclability of both 3D-TTA and 2D-TTA in the first 10 cycles is considerably good. The generation of Cu_6Sn_5 was somewhat different from Tamura's previous report in which the intermetallic compound layers were formed by heat treatment [20]. In Tamura's article the cyclability was good in the first 20 cycles, but deteriorated in the following cycles. The XRD pattern of 3D-TTA after 10 cycles shown in Fig. 4B indicates that the Cu_6Sn_5 phase was inherited probably after cycles.

The thickness of tin film is merely around 500 nm which also reduces volume expansion and improve adhesion strength between active material and substrate. Moreover, in 3D-TTA the uniform tin microflake structure (seen in Fig. 3a1) of 500 nm thickness formed on the rough surface of copper branches provides appropriate space for tin to expand in either upper or side directions so that it could strongly bind to the substrate under about 360% volume expansion. However, in 2D-TTA the tin film did not form microflake structure but pulverized severely. Huge stress–strain caused by volume change accumulated along the flat copper foil and led ultimately to the electrode failure while the stress–strain released on the rough surface of copper branches and resulted in the well-behaved microflake structure. High rate cycling capability of 3D-TTA is attributed to microflake structure and the thin tin film deposited over the whole surface of copper branches, which provide more active sites and short transfer distance for rapid lithiation/delithiation. Besides, the 3D conductive and stretchy network structure would also be favorable to the good cyclability and high rate capability [13].

To further understand the reason for the good cyclability of 3D-TTA, EIS measurements were conducted after charging the electrodes up to 1.5 V (vs. Li/Li^+), a namely 100% delithiation state. The EIS graphs after 1st, 10th, 20th, 30th and 40th cycles are presented in Fig. 5. The Nyquist plots all comprise two semicircles in high-frequency (HF) and medium-frequency (MF) ranges and a line inclined at an approximate 45° angle to the real axis in low frequency. According to the previous studies [22,23], the HF semicircle is ascribed to SEI film, the MF semicircle to interfacial charge-transfer and the linear part to Li^+ diffusion process within electrode. As discussed above, CV result suggests that SEI film formed only in the 1st charge process and retained in the

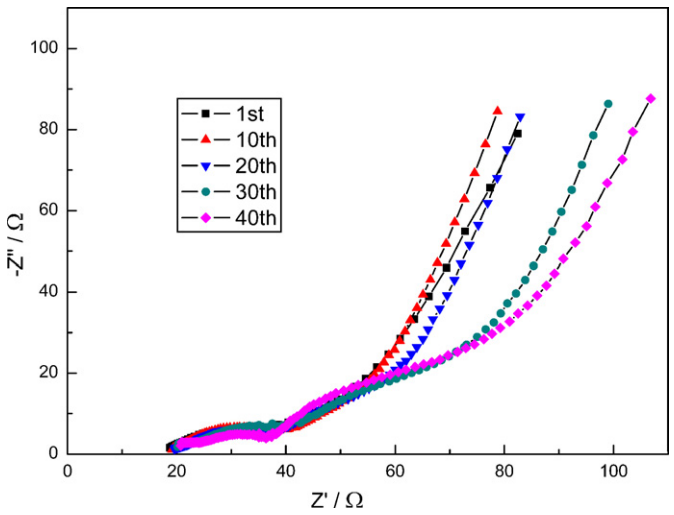

Fig. 5. Electrochemical impedance spectroscopies of 3D-TTA after 1st, 10th, 20th, 30th and 40th cycles.

following cycles, so the HF resistance has little change. The MF resistance keeps almost similar before the 20th cycle. It suggests the structure of 3D-TTA is highly stable, which corresponds to the good cyclability that the capacity retention reaches 97% after 20 cycles. However, the MF resistance changes slightly in the 30th and maintains similar in the 40th cycle. It probably associates with tin film's cracking into microflakes and some pulverization due to the cyclic expansion of crystal structure, which lead to increase of contact resistance between active materials and hinder interfacial charge-transfer. This can also be confirmed from the cycling performance in Fig. 2a, in which the capacity fades after the 30th cycle due to the microstructure changes of the electrode.

4. Conclusions

A 3D tin thin-film anode was successfully prepared by electroless plating and applied in lithium-ion batteries. Tin distributed both inside and outside the copper hollow branches and the thickness of tin film was around 500 nm. X-ray diffraction demonstrated that Cu_6Sn_5 phase was formed between tin and copper substrate, which strengthened the bonding force between active materials and substrate. Furthermore, the well-behaved microflake structure also restrained tin's shedding from the current collector. Although 3D-TTA displayed only 72% initial columbic efficiency, it showed good cycling performance with capacity retention 97% after 20 cycles and 84% after 40 cycles, which would be potential electrode in commercial lithium-ion batteries.

Acknowledgements

This work was supported by the National Natural Science Foundation of China (50574008, 50954005), National Basic Research Program of China (2007CB936502) and National 863 Program (2006AA03Z230, 2008AA03Z208).

References

[1] M. Winter, R.J. Brodd, Chem. Rev. 104 (2004) 4245.
[2] M. Winter, J.O. Besenhard, Electrochim. Acta 45 (1999) 31.
[3] S. Yang, P.Y. Zavalij, M.S. Whittingham, Electrochem. Commun. 5 (2003) 587.
[4] W. Choi, J.Y. Lee, B.H. Jung, H.S. Lim, J. Power Sources 136 (2004) 154.
[5] M. Inaba, T. Uno, A. Tasaka, J. Power Sources 146 (2005) 473.
[6] H. Morimoto, S. Tobishima, H. Negishi, J. Power Sources 146 (2005) 469.
[7] L. Balan, R. Schneider, J. Ghanbaja, P. Willmann, D. Billaud, Electrochim. Acta 51 (2006) 3385.
[8] S.H. Ju, H.C. Jang, Y.C. Kang, J. Power Sources 189 (2009) 163.
[9] C. Arbizzani, S. Beninati, M. Lazzari, M. Mastragostino, J. Power Sources 141 (2005) 149.
[10] M. Yoshio, T. Tsumura, N. Dimov, J. Power Sources 146 (2005) 10.
[11] J.Y. Xiang, J.P. Tu, X.L. Wang, X.H. Huang, Y.F. Yuan, X.H. Xia, Z.Y. Zeng, J. Power Sources 185 (2008) 519.
[12] L. Huang, H.B. Wei, F.S. Ke, X.Y. Fan, J.T. Li, S.G. Sun, Electrochim. Acta 54 (2009) 2693.
[13] T. Jiang, S. Zhang, X. Qiu, W. Zhu, L. Chen, Electrochem. Commun. 9 (2007) 930.
[14] G.J. Davies, S. Zhen, J. Mater. Sci. 18 (1983) 1899.
[15] W. Pu, X. He, J. Ren, C. Wan, C. Jiang, Electrochim. Acta 50 (2005) 4140.
[16] H. Guo, S. Zhao, H. Zhao, Y. Chen, Electrochim. Acta 54 (2009) 4040.
[17] P.A. Connor, J.T.S. Irvine, Electrochim. Acta 47 (2002) 2885.
[18] M. Martos, J. Morales, L. Sánchez, Electrochim. Acta 46 (2000) 83.
[19] G.X. Wang, J. Yao, H.K. Liu, S.X. Dou, J. Ahn, Electrochim. Acta 50 (2004) 517.
[20] N. Tamura, R. Ohshita, M. Fujimoto, S. Fujitani, M. Kamino, I. Yonezu, J. Power Sources 107 (2002) 48.
[21] N. Tamura, R. Ohshita, M. Fujimoto, M. Kamino, S. Fujitani, J. Electrochem. Soc. 150 (2003) A679.
[22] S. Yang, H. Song, X. Chen, Electrochem. Commun. 8 (2006) 137.
[23] S. Yang, H. Song, X. Chen, J. Power Sources 173 (2007) 487.